A Dynamic Snow Depth Inversion Algorithm Derived From AMSR2 Passive Microwave Brightness Temperature Data and Snow Characteristics in Northeast China

Yanlin Wei, Xiaofeng Li, *Member, IEEE*, Lingjia Gu, *Member, IEEE*, Xingming Zheng, *Member, IEEE*, Tao Jiang, *Member, IEEE*, Xiaojie Li, *Member, IEEE*, and Xiangkun Wan

***Abstract*—Snow cover plays an important role in climate, hydrology, and ecosystem. At present, passive microwave remote sensing is the most effective method for monitoring global and regional snow depth (SD). The traditional SD inversion algorithms use empirical or semiempirical methods to establish a fixed relationship between the SD and brightness temperature difference, given snow particle size and snow density. However, the snow characteristics present large temporal heterogeneity in Northeast China, and it leads to the inadaptability of the SD retrieval algorithm; using a fixed empirical coefficient will lead to large errors in SD inversion. In this study, a novel dynamic method was proposed to retrieve SD based on AMSR2 brightness temperature data. A snow survey experiment was designed to collect snow characteristics in different periods in Northeast China, and the microwave emission model of layered snowpacks was applied to simulate brightness temperature with varying snow characteristics to determine the dynamic coefficients in the SD retrieval algorithm. The validation results at 98 meteorological stations demonstrate that the novel dynamic SD inversion algorithm achieved better stability in the long-term sequence, its RMSE, bias, and *R* are 7.79 cm, 1.07 cm, and 0.61, respectively. Furthermore, compared with Che SD products, Chang algorithm, and AMSR2 SD products, the novel algorithm can obtain specific dynamic coefficients considering the snow metamorphism and has a higher accuracy of SD inversion in the whole winter. In conclusion, this novel SD inversion algorithm is more applicable and accurate than the existing SD inversion products in Northeast China.**

***Index Terms*—Dynamic algorithm, northeast China, passive microwave, snow depth (SD).**

Manuscript received November 2, 2020; revised March 2, 2021 and April 20, 2021; accepted May 7, 2021. Date of publication May 13, 2021; date of current version May 27, 2021. This work was supported in part by the National Natural Science Foundation of China under Grant 41871248 and Grant 41871225, in part by the Project of Jilin Province Development and Reform Commission under Grant 2021C044-7, and in part by the Basic Resources Survey Project of National Science and Technology—The investigations on the characteristics and distribution of snow in China under Grant 2017FY100501. *(Corresponding authors: Xiaofeng Li; Lingjia Gu.)*

Yanlin Wei, Xiaofeng Li, Xingming Zheng, Tao Jiang, Xiaojie Li, and Xiangkun Wan are with the Northeast Institute of Geography and Agroecology, Chinese Academy of Sciences, Changchun 130102, China (e-mail: weiyl18@mails.jlu.edu.cn; lixiaofeng@iga.ac.cn; zhengxingming@iga.ac.cn; jiangtao@iga.ac.cn; lixiaojie@iga.ac.cn; wanxiangkun@iga.ac.cn).

Lingjia Gu is with the College of Electronic Science and Engineering, Jilin University, Changchun 130012, China (e-mail: gulingjia@jlu.edu.cn).

Digital Object Identifier 10.1109/JSTARS.2021.3079703

I. Introduction

SNOW cover plays an essential role in the global hydrological cycle, and it is one of the main supply sources for rivers and groundwater [1]–[4]. The high reflectivity of the snow surface and the adiabatic effect of the snow layer significantly affect global energy cycle processes [5]. Snow depth (SD) is a significant parameter in climate and hydrologic model simulations [6]. Therefore, the accurate estimation of SD is crucial for understanding climate systems and managing water resources in cold regions [7].

In recent decades, substantial efforts have been made to develop applicable snow cover observations. Since the 1970s, passive microwave remote-sensing sensors have evolved, passive microwave can penetrate clouds, independent of the weather, and interact with the snowpack [8]–[14]. Passive microwave remote sensing is the most effective method for measuring snow cover at the global and regional scales [15]–[17]. Deeper snow layers provide more snow crystals to enhance the scattering ability of the snowpack with the result that microwave energy is away from the sensor. Hence, the brightness temperatures are generally lower for deep snowpacks and higher for shallow snowpacks. Based on this fact, the international mainstream SD inversion algorithm was first proposed by Chang *et al*. [18], which takes the advantage of the brightness temperature difference (TBD) between 36 (or 37 GHz) and 18 GHz (or 19 GHz) to obtain a linear SD inversion algorithm.

Currently, studies have shown that the prior knowledge of snow properties is important in estimating SD from passive microwave data [19]–[23]. SD retrieved from passive microwave remote-sensing data can be influenced by the snowpack properties, such as snow particle size and density. It has been reported that snow conditions, especially snow grain size, determine the coefficient of the spectral gradient for the linear SD inversion algorithm. The traditional empirical and semiempirical algorithms are based on a fixed snow density and snow particle size, and calibrate the relationship between SD and TBD on limited datasets; few researchers considered snow metamorphism and gave a dynamic relationship between SD and TBD only based on a simple empirical algorithm. For example, the coefficient was 1.59 for Chang's algorithm when grain size was 0.3 mm [18],

and the coefficient was 0.78 for Foster's algorithm when grain size was 0.40 mm [24]. Josberger and Mognard [25] reported that the TBD between 36 and 18 GHz continued to increase due to snow metamorphism with time when the snow thickness was constant. Thinner snow grains cause decreased microwave scattering, which leads to an underestimating SD result. Thus, it is necessary to consider the effects of snow cover evolution on the regression coefficients of the algorithm. Che *et al*. [26] modified the algorithm coefficient based on Chang's algorithm and developed a regional SD inversion algorithm in China, but the changes in snow characteristics were not considered. Kelly [27] developed a dynamic SD algorithm by introducing a dynamic coefficient that reflected changes in snow particle size; however, it was not applicable for Northeast China because it always seriously overestimated the measured SD [28]. All arguably are not able to work with the same accuracy with evolving snow characteristics.

In addition, vegetation, especially forests, affects the passive microwave radiation signal. Not only the forest canopy affects the upwelling radiation signal in the snowpack but the forest itself emits radiation, which can cause serious errors in the inversion results [29]–[32]. Therefore, there exists a serious challenge for SD inversion in Northeast China as forest cover is more than 30% in the region. SD inversion in forested areas has been widely concerned by many scholars. Foster *et al*. [24] introduced forest parameters to improve the underestimation of the forest area inversion SD; however, it was found that the inversion accuracy of Foster's algorithm could not meet SD inversion requirements in forest area [28]; Che *et al*. [29] used the optimal iterative method to calculate forest transmissivity based on the microwave emission model of layered snowpacks (MEMLS) radiative transfer model and established an SD lookup table for the forest region in Northeast China. Although this method obtained more accurate results compared with the traditional empirical inversion algorithm, it required more snow parameters that were difficult to obtain, and it was not conducive to SD inversion on large scale.

Although there have been many studies on SD inversion, few studies considered both the influence of snow metamorphism and forest attenuation in an empirical SD inversion algorithm based on the relationship between SD and TBD. In this work, a dynamic coefficient was quantified to establish a dynamic SD algorithm; the purpose was to consider the change of the snow characteristics throughout the winter and reduce the effect of snowpack evolution on the accuracy of SD estimations. Besides, the forest fraction was also introduced and optimized to correct forest attenuation in forest areas. Eventually, a dynamic SD inversion algorithm for considering snow metamorphism and forest attenuation was derived, which was called "the Northeast Institute of Geography and Agroecology Snow (IGAS) depth inversion algorithm." In contrast to complex physical models, the IGAS algorithm does not require to input any snow parameter; all independent variables in the IGAS algorithm can be easily acquired using passive microwave remote-sensing technology, making rapid, efficient, and massive operations possible. Compared with the traditional empirical algorithms, the IGAS algorithm considered both snow evolution and forest attenuation by a specific dynamic coefficient, and a higher SD inversion accuracy was achieved. In this article, the study area and data are introduced in Section II. In Section III, we describe the derivation process for the IGAS algorithm. The results and analysis are described in Section IV. Factors influencing the accuracy of the IGAS inversion algorithm are discussed in Section V. Finally, Section VI presents the conclusions with the entire study in this article.

TABLE I
AMSR2 SENSOR PARAMETERS

Frequency: Footprint (GHz):(km × km)	6.9	35x62
	7.3	35x62
	10.65	24x42
	18.7	14x22
	23.8	15x26
	36.5	7x12
	89	3x5
Polarization Type	V, H	
Data acquisition	Daily	
Time series	5/2012-present	
Incidence angle (degrees)	55	

II. STUDY AREA AND DATA

A. Study Area

Northeast China is sensitive to global climate change and is also an important agricultural base in China [33], [34]. Therefore, the research on snow monitoring in Northeast China is significant for understanding changes in the regional environment and sustainable agriculture development. According to the International Geosphere–Biosphere Program (IGBP) classification system in Northeast China, farmland and grassland cover represents over 60% of the total area. The forest covers 30% of the total area. Rivers, lakes, residential areas, and other areas cover the remaining 10% [see Fig. 1(a)]. In addition, Li *et al*. [35] proposed a snow cover classification method in China based on a binary system of the three climate variables proposed by Sturm *et al*. [36]. The results showed that the snow cover in Northeast China could be classified into five types, including prairie, taiga, tundra, mountain, and ephemeral types. Different types of snow cover in Northeast China had characteristics that differed from the Sturm–Holmgren–Liston classification. The diversity of snow types in Northeast China indicated that the characteristics of snow cover were different from the other areas.

B. AMSR2 Data

AMSR2 is a new type of sensor that followed AMSR-E, and it is mounted on the global change observation mission first–Water "SHIZUKU" satellite launched by Japan in May 2012. The sensor has 14 channels at seven frequencies: 6.9, 7.3, 10.65, 18.7, 23.8, 36.5, and 89 GHz (see Table I). Each frequency has dual polarizations, which are horizontal and vertical. The AMSR2 L3 level brightness temperature data were released with 25 km resolution by the JAXA, and it could be acquired from

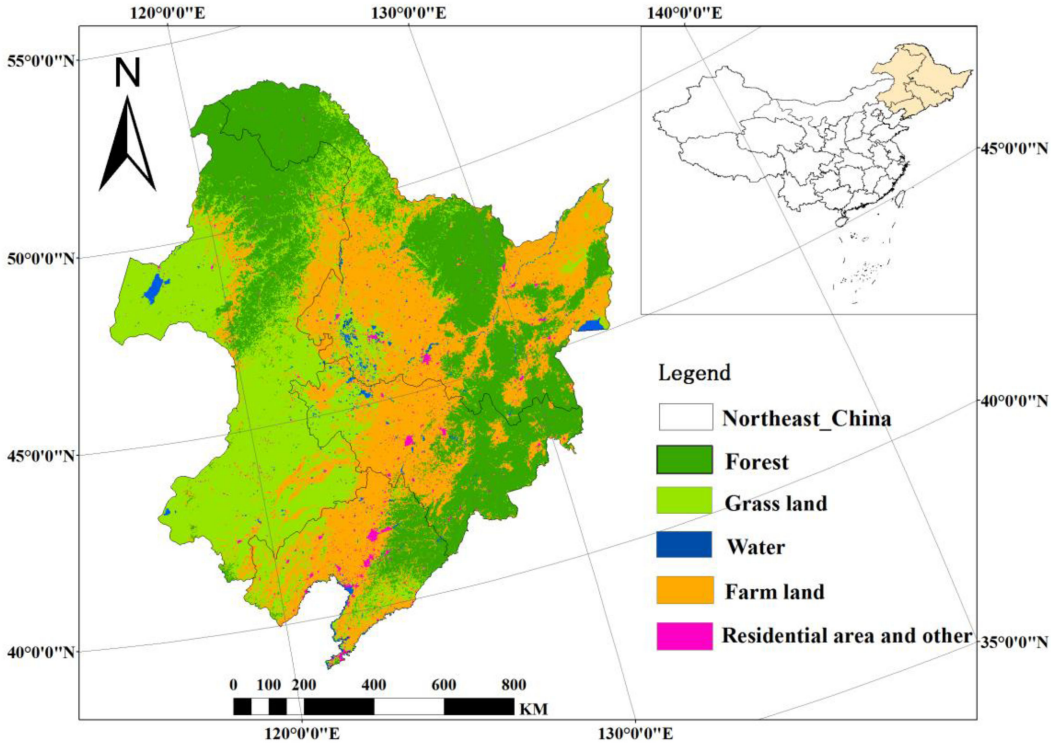

(a)

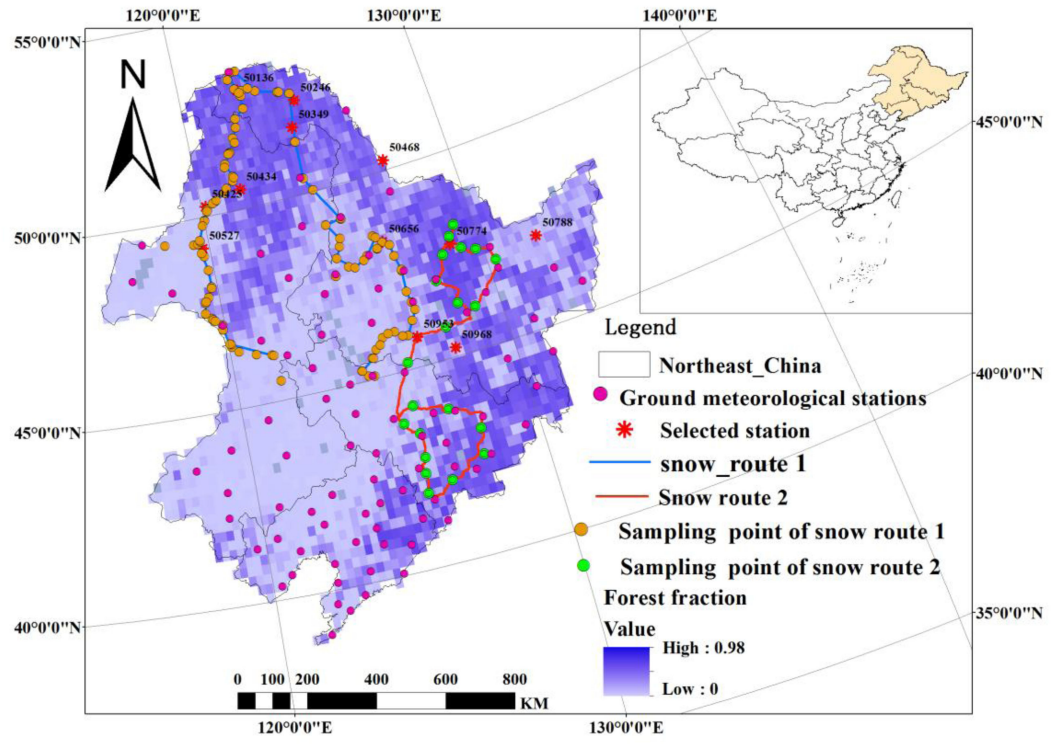

(b)

Fig. 1. Study area is located in Northeast China. (a) Land cover distribution of the study area. (b) Forest fraction within each AMSR2 pixel calculated from the MCD12Q1 data, and different colors represent the distribution of sampling points on the survey route and meteorological stations.

TABLE II
STATISTICAL RESULTS OF SNOW CHARACTERISTICS DATA IN NORTHEAST CHINA

	Snow density(g/cm^3)		**Snow grain size**(mm)		**Snow depth**(cm)	
Data	Range	Mean	Range	Mean	Range	Mean
Dec	0.07-0.15	0.10	0.74-2.54	1.96	4.48-19.67	13.97
Jan	0.10-0.14	0.11	0.92-3.42	2.45	7.33-23..96	14.68
Feb	0.11-0.20	0.12	1.41-3.10	2.67	7.68-50.68	17.83
Mar	0.12-0.21	0.14	1.28-5.13	3.42	5.81-32.66	15.78

the JAXA website at.[1] Using the geographical coordinates of the meteorological station, the pixel brightness temperature data at the station were extracted and prepared for further validating analysis from December 2013 to February 2018. To avoid the impact of snowmelt on brightness temperature, the AMSR2 L3 level nighttime data (descending orbits) was downloaded in this article.

C. Auxiliary Data

MODIS land cover type data (MCD12Q1) were used in this article. The MCD12Q1 product with a spatial resolution of 500 m could be downloaded from the site at.[2] We reclassify MCD12Q1 data into five categories based on the IGBP classification system [37], including farmlands, forests, grasslands, water, and residential area, and others [see Fig. 1(a)]. In the experiment, the forest fraction (ff) was determined according to each grid cell in the MCD12Q1 data within each AMSR2 passive microwave pixel footprint [see Fig. 1(b)].

D. Ground Observations

1) Snow Survey Routes Datasets (Dataset 1): Dataset 1 was used to establish a novel algorithm. The snow characteristics data were acquired based on the field campaign supported by the Chinese snow survey project from December 2017 to March 2018. During the field experiment period, two snow survey routes were designed [see Fig. 1(b)] in Northeast China, and a large number of snow samples were measured, included 74 samples in nonforest areas and 87 samples in forest areas. These measurements included SD, snow density, snow grain size, and the stratigraphy of the snowpack. All snow cover parameters (SD, snow density, and snow particle size) and environmental parameters (air temperature, snow layer temperature, and surface temperature) were measured using the same instrument and method [38]. Table II lists the details of the snow survey routes data, including SD, snow density, and snow grain size.

2) Meteorological Station Datasets (Dataset 2): The meteorological stations' data were obtained from the National Meteorological Information Centre, China Meteorology Administration.[3] The recorded variables include the site name, observation time, geolocation (latitude and longitude), elevation (m), and SD (cm), which are applied to validate the retrieved SD based on the novel algorithm. Dataset 2 covers 98 stations throughout Northeast China from December 2013 to February 2018 [see Fig. 1(b)]. A total of 33 174 independent samples were collected during the period December 2013–February 2018. Furthermore, the SD from 14 meteorological stations was selected to illustrate the seasonal variations in the retrieved and observed SD, including seven stations in nonforest areas and seven in forest areas.

E. Existing SD Inversion Algorithms and SD Products

Chang *et al*. [18] assumed that the snow crystals were spherical particles, snow density was 0.3 g/cm^3, and snow particle size was 0.3 mm. Based on the theoretical calculations, empirical studies developed an algorithm for passive microwave remote sensing. The following algorithm was applicable:

$$\mathrm{SD} = A_0 \times (\mathrm{Tb}_{19\mathrm{H}} - \mathrm{Tb}_{37\mathrm{H}}) \tag{1}$$

where SD represents the snow depth (cm), $A_0 = 1.59$, which is the calibration parameter based on a fixed snow density and snow particle size. $\mathrm{Tb}_{19\mathrm{H}}$ and $\mathrm{Tb}_{37\mathrm{H}}$ are the brightness temperatures at 19 GHz and 37 GHz in the horizontal polarization, respectively.

Che *et al*. [26] refined the retrieval coefficient of Chang's algorithm by observed SD from Chinese ground stations and established SD products based on the passive microwave remote-sensing data (SMMR from 1978 to 1987 and SMM/I from 1987 to 2019) in China [39]. Che SD product could be downloaded from the site at.[4]

The current AMSR2 SD product was generated from the original AMSR-E algorithm. The brightness temperatures for different channels were checked to determine if the snow layer was likely to be shallow or medium-to-deep [40]. If the snow layer was detected but was likely to be shallow, the SD was estimated to 5.0 cm. For medium-to-deep snow, the algorithm separately retrieved SD for the forested and nonforested fractions, and combined them to obtain the total SD within each AMSR2 pixel; the more detailed introduction was given in [27]. The AMSR2 SD product was acquired from the JAXA website at.[5]

[1][Online]. Available: https://gcom-w1.jaxa.jp
[2][Online]. Available: https://search.earthdata.nasa.gov
[3][Online]. Available: http://data.cma.cn/en
[4][Online]. Available: http://data.tpdc.ac.cn
[5][Online]. Available: https://gcom-w1.jaxa.jp

III. Methodology

A. Radiative Transfer Model

The MEMLS radiative transfer model characterizes the radiative properties of the snowpack layer based on the physical properties [41]. Its advantage is that it has a wide frequency range (5–100 GHz) and high simulation efficiency. The MEMLS model uses a six-stream approximation theory to calculate the volume scattering in snowpack and can calculate the brightness temperature that is radiated from snowpack [42], [43]. The snow correlation length is used to describe the scattering of snow layers in the MEMLS model [44], and it is defined as the inverse of the derivative of the autocorrelation function of snow structure at zero displacements [21]. In this study, according to Davis and Dozier [45], the correlation length was related to snow grain size and snow density, and it could be calculated by (2) and (3), which was described in [21] and [44]–[46]

$$P_c = (4 \times \rho/\rho_i \times (1 - \rho/\rho_i)/S) \tag{2}$$

$$S = 2 \times a/n \tag{3}$$

where P_c is the correlation length, ρ is the snow density, ρ_i represents the ice density (917 kg/m^3), S is the ice surface area per unit volume, a is the side length of the cubic box, and n is the number of particles along with its one. According to the field measurements, the snow particle is similar to the pillar; thus, we used the measured snow grain size, as the long side length and the short side length were randomly selected to be between two-third and one time the long side length; it was assumed that these numbers (1000) were homogeneously distributed within a cubic box, and the volume of the cubic box could be calculated according to snow density and the volume of particles [21], [46].

B. Quantifying Dynamic Coefficient Based on MEMLS and Snow Characteristics

To establish a dynamic relationship between TBD and SD through a dynamic coefficient that reflects the change in snow cover characteristics, it is necessary to obtain snow characteristics data in different periods. Therefore, a field snow survey experiment was conducted from December 2017 to March 2018. Snow characteristics in nonforest from dataset 1, including snow grain size, snow density, and SD, were analyzed in four periods, and the results were given in Table II, which illustrated the difference of snow characteristics in time.

The procedure for quantifying the dynamic coefficient was shown in Fig. 2. First, the measured snow characteristics in different periods, a total of 74 samples, were used as input parameters for the MEMLS model, then the MEMLS model was used to simulate brightness temperature at 18 GHz and 36 GHz, respectively. By repeating operations based on snow characteristics at different periods, a TBD dataset was obtained.

We then defined a dataset C_M, which was expressed as

$$C_M = \mathrm{TBD_H}/\mathrm{SD} \tag{4}$$

where $\mathrm{TBD_H}$ represents a brightness temperature difference dataset between 18 and 36 GHz at horizontal polarization, so it was calculated based on MEMLS, and also changing with the snow characteristics; SD as the input snow depth in the MEMLS model, so it was obtained through field experiments; C_M means the relationship between $\mathrm{TBD_H}$ and SD [18], as (4), and it was also dynamical changing with snow characteristics, its range of value represented the dynamic coefficient.

The range of the C_M value could be obtained based on the study above. To quantify the dynamic coefficients, a relationship between $\mathrm{TBD_V}$ and C_M was established through regression. The result was shown in Fig. 3, and it could be found that $\mathrm{TBD_V}$ and C_M conformed to the form of tenth power; so, the relationship was determined as (5), and the correlation coefficient R was

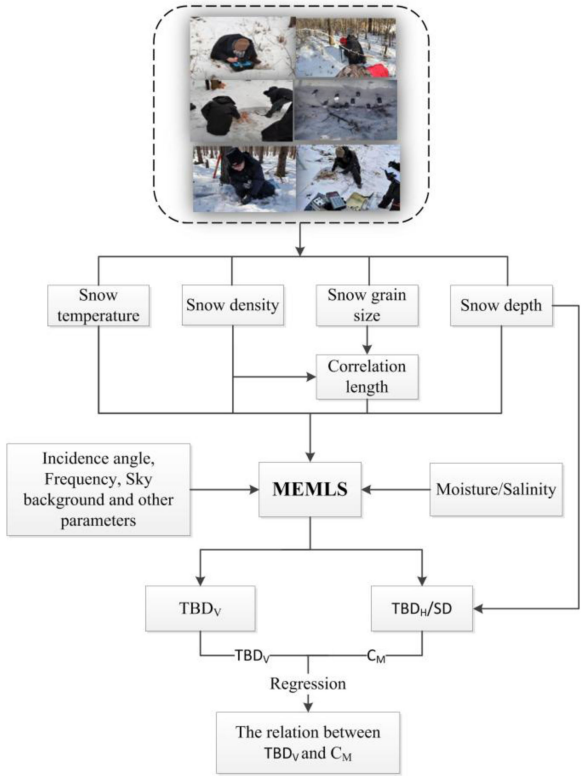

Fig. 2. Flowchart for quantifying dynamic coefficient based on the MEMLS and snow characteristics.

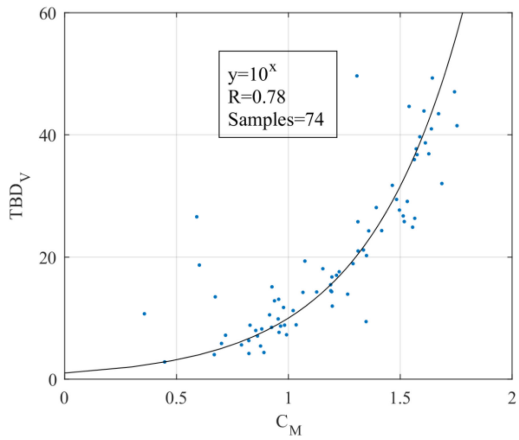

Fig. 3. Scatter plots $\mathrm{TBD_V}$ and C_M.

0.74

$$\mathrm{TBD_V} = 10^{C_M}. \tag{5}$$

Considering C_M that can be determined via (5), its specific expression can be derived using the following:

$$C_M = \log_{10}\mathrm{TBD_V}. \tag{6}$$

Finally, the dynamic SD inversion algorithm can be derived by introducing (4) into (6)

$$\mathrm{SD} = \mathrm{TBD_H}/\log_{10}\mathrm{TBD_V} \tag{7}$$

where $\mathrm{TBD_H} = \mathrm{Tb_{18H}} - \mathrm{Tb_{36H}}$; similarly, $\mathrm{TBD_V} = \mathrm{Tb_{18V}} - \mathrm{Tb_{36V}}$; SD was the retrieved snow depth based on the brightness temperature that was simulated through MEMLS. In fact, AMSR2 passive microwave brightness temperature data can be used directly to replace TBD in (7) in the actual SD inversion.

C. IGAS SD Inversion Algorithm

In addition to the impact of snowpacks evolution on the accuracy of SD estimations, the forest can also attenuate microwave radiation from snowpack, and its upwelling radiation contributes to passive microwave data observed by satellites [30], [31]. Forest covers more than 30% of Northeast China [see Fig. 1(a)]. If the effects of forest radiation signals are not eliminated, the SD inversion result will have serious errors. Foster *et al.* [24] introduced forest fraction parameters $(1/(1-\mathrm{ff}))$ to remove the forest canopy attenuation of snowpack radiation. However, the retrieved SD by Foster's algorithm always overestimated the observed SD in Northeast China [28], which might cause by the following reasons: First, the metamorphism of the snowpack was not considered. Second, when ff was closer to 1, the retrieved SD by Foster's algorithm approached infinity, which lost effectiveness for the area with large forest coverage. Therefore, based on Foster's study, this study uses an optimal algorithm to reduce the attenuation of the snowpack signal by the forest canopy. The optimal SD inversion algorithm for forest areas is expressed as follows:

$$\mathrm{SD_{forest}} = \left(\frac{\mathrm{TBD_H}}{1 - a \times \mathrm{ff}}\right) \Big/ \log_{10}\left(\frac{\mathrm{TBD_V}}{1 - b \times \mathrm{ff}}\right) \tag{8}$$

where ff is the forest fraction; it can be obtained from MODIS land cover type data (MCD12Q1); the range of value is from 0 to 1 within a spatial resolution of 25 km; and a and b are the calibration coefficients.

The value of a and b was obtained by an optimization scheme in this study, and it is dependent on the forest fraction (see Section V). The range of forest fraction was evenly distributed between 0.1 and 1 in snow sampling data; thus, the value of a and b was calculated based on 87 snow samples in the forest region from dataset 1. The results showed that the error value between the inversion and the observed SD was the smallest when the value of a was found to be 0.4 and b was equal to 0.6; therefore, the value of a and b was taken as 0.4 and 0.6 in this article, respectively. A more detailed process can be found in Section V. Finally, the SD inversion algorithm for considering snow metamorphism and forest attenuation, called IGAS, can be described as the following:

$$\mathrm{SD_{IGAS}} = \left(\frac{\mathrm{TBD_H}}{1 - 0.4 \times \mathrm{ff}}\right) \Big/ \log_{10}\left(\frac{\mathrm{TBD_V}}{1 - 0.6 \times \mathrm{ff}}\right). \tag{9}$$

TABLE III
STEPS TO DISTINGUISH SNOW FROM PRECIPITATION, COLD DESERT, FROZEN GROUND, AND WET SNOW

Steps	Conditions for AMSR2
1.Scattering signature	Tb_{18V}-Tb_{36V} > 0K
2. Precipitation	Tb_{23V} > 259 K or 254 K ⩽ Tb_{23V} ⩽ 258 K and Tb_{18V} – Tb_{36V} ⩽ 2 K
3. Cold desert	Tb_{18V} – Tb_{18H} ⩾ 18 K and Tb_{18V} – Tb_{36V} ⩽ 10 K and Tb_{36V} – Tb_{89V} ⩽ 10 K
4. Frozen ground	Tb_{18V} – Tb_{18H} ⩾ 8 K and Tb_{18V} – Tb_{36V} ⩽ 2 K and Tb_{23V} – Tb_{89V} ⩽ 6 K
5. Wet snow	Tb_{36V} – Tb_{36H} ⩾ 10 K

D. Snow Identification

Deserts, frozen soils, and precipitation have similar scattering characteristics to snow cover. To improve the accuracy of the SD inversion algorithm, the impacts of cold desert, frozen ground, and precipitation scatterers should be eliminated before estimating SD based on the IGAS algorithm in Northeast China. We used the Grody, Kelly, and Walker [27] methods to remove the effects of scatterers before the SD inversion in this study. The discriminated methods are given in Table III.

IV. RESULTS

The IGAS algorithm was evaluated using dataset 2. Meanwhile, to demonstrate the performance of the IGAS algorithm, it was compared with three other operational satellite SD algorithms and products.

A. Comparison of SD With Meteorological Stations

Dataset 2, including 33 174 samples during the period December 2013–February 2018, was used to further analyze the applicability and deficiency of the IGAS algorithm in Northeast China. The color-density scatterplots between the retrieved and observed SD were illustrated in Fig. 4, and it shows that the high frequency of SD is mainly distributed around 1:1 line, but we found that there are few data away from it, especially for deeper snow cover. This phenomenon would be discussed in detail in Section V. In addition, the retrievals of the IGAS algorithm tend to be overestimated in terms of bias by approximately 1.07 cm, but it showed good performance against observed SD in long term, and the overall RMSE and *R* were 7.79 cm and 0.61, respectively.

Forest correction was still one of the main challenges in SD estimations over forested areas [31]. Thus, retrieval sensitivity

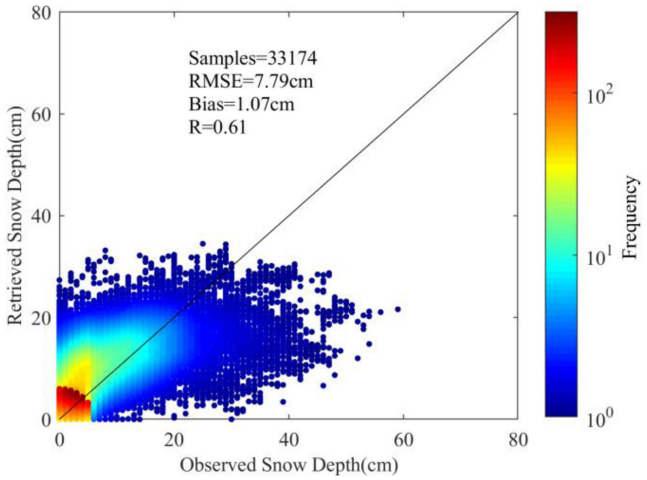

Fig. 4. Color-density scatterplots of the estimated and observed SD at 98 meteorological stations from 2013 to 2018.

to land cover types (nonforest and forest) was considered in this study. Any pixel where the land cover fraction is greater than 85% was viewed as a pure land cover type [19]. A total of 18 321 independent samples were located in nonforest areas, and the other 14 853 independent samples were located in forest areas. Fig. 5(a) and (b) showed the validation results of the IGAS algorithm against meteorological station observations in different land cover types, respectively. The IGAS algorithm showed better performance in nonforest areas [see Fig. 5(a)], and the overall RMSE, bias, and R were 6.43 cm, 2.43 cm, and 0.69, respectively. Fig. 5(b) illustrated that the most serious estimate errors occurred in forest areas, its RMSE and R were 9.20 cm and 0.47 in here; it implied that the effects of forest canopy on the microwave signal still had significant impacts on the IGAS algorithm, and the reason would be discussed in detail in Section V.

B. Comparison With the Existing Snow Products

In this article, 14 meteorological stations were also randomly selected to illustrate the seasonal variations in the retrieved and observed SD, and seven stations were located in the nonforest areas, the other stations were located in forest areas, and their spatial distribution was shown in Fig. 1(b). Besides, the retrieved SD based on the IGAS algorithm was compared with the other three SD algorithms and products (Che product, Chang algorithm, and AMSR2 SD product).

The seasonal consistency between retrieved based on IGAS algorithm and observations at 14 meteorological stations was shown in Fig. 6. It can be found that the inversion results of the IGAS algorithm had good agreement with observed SD at 14 meteorological stations, respectively, although the inversion result had a large error with observed SD in a special period, such as station 50 778 in 2015 and station 54 276 in 2017; the IGAS algorithm had high stability in the long-term sequence from the overall result. In addition, we also compared the accuracy of four SD algorithms and products based on 14 meteorological stations' data, and the result was shown in Fig. 7; it represented the error frequency distribution of retrieved SD, which equals the observed SD minus the retrieved SD. It can be found that the existing algorithms and products, including Che SD product, Chang algorithm, and AMSR2 SD product, had instability in the long term, they produced larger errors, and their RMSEs exceeded 10 cm. The Chang algorithm that assumed snow grain size was a constant (0.3 mm) throughout the winter; however, according to the field observation data in Northeast China, the snow grains size varied greatly in different periods and was much larger than 0.3 mm (see Table II); as a result, the Chang algorithm had a high uncertainty in Northeast China, its RMSE and R were 17.71 cm and 0.12, respectively. Although the AMSR2 SD product considered the growth of snow grain size over time, it was found that there was no improvement compared with the Chang algorithm in Northeast China; on the contrary, it showed bad performance against the Chang algorithm, its RMSE and R were 31.16 cm and 0.08, and it seriously overestimated the observed SD in terms of bias, so it could not effectively monitor SD in Northeast China. The Che product was superior to the other two products with R and RMSE of 0.26 and 10.87 cm, respectively. For the IGAS algorithm, the error range was evenly distributed between -10 and 10 cm, and the performance of the IGAS algorithm was best among the four snow algorithms and products with RMSE and bias were 7.73 cm and -0.15 cm, respectively. Although the IGAS algorithm had higher reliability and stability in the long term with an R of 0.46, it was more suitable as an SD inversion algorithm in Northeast China.

V. Discussion

The validation results showed that the IGAS algorithm had higher accuracy for SD inversion than the existing products and algorithms. The advantage of the IGAS algorithm was that it considered the change in snow characteristics and produced higher inversion accuracy. However, the IGAS algorithm was also affected by some factors.

A. Impacts of Different Snowfall Periods

Snow properties evolved with time. Table II illustrated that the snow characteristics of old and new snow cover, such as snow density and snow grain size, were quite different. Therefore, the impacts of snow metamorphism with time on the inversion result should be considered when performing SD inversion. This section mainly discussed the accuracy of the IGAS algorithm on different snow periods. From observation data obtained in the meteorological station, it could be found that snowfall times in Northeast China mainly occur in four months (December, January, February, and March), namely I, II, III, and IV, as shown by the black line in Fig. 8. Meanwhile, we also noticed that the error (blue line in Fig. 8) between the retrieved SD based on the IGAS algorithm and the observed SD on the meteorological station had obvious changes in four snowfall periods. The results showed that the error gradually increased with the snowfall time and reached the maximum in March.

To better describe the influence of snow cover metamorphism on the SD inversion accuracy, the data of the above 14 meteorological stations were selected as the observed SD

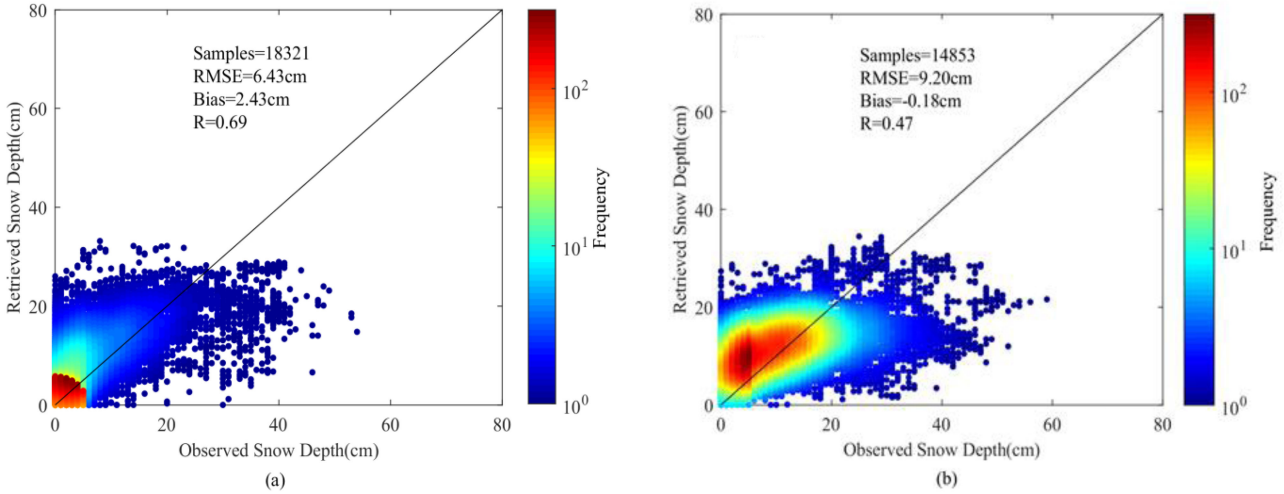

Fig. 5. Color-density scatterplots of estimated and observed SD at meteorological stations from 2013 to 2018. (a) Nonforest regions. (b) Forest regions.

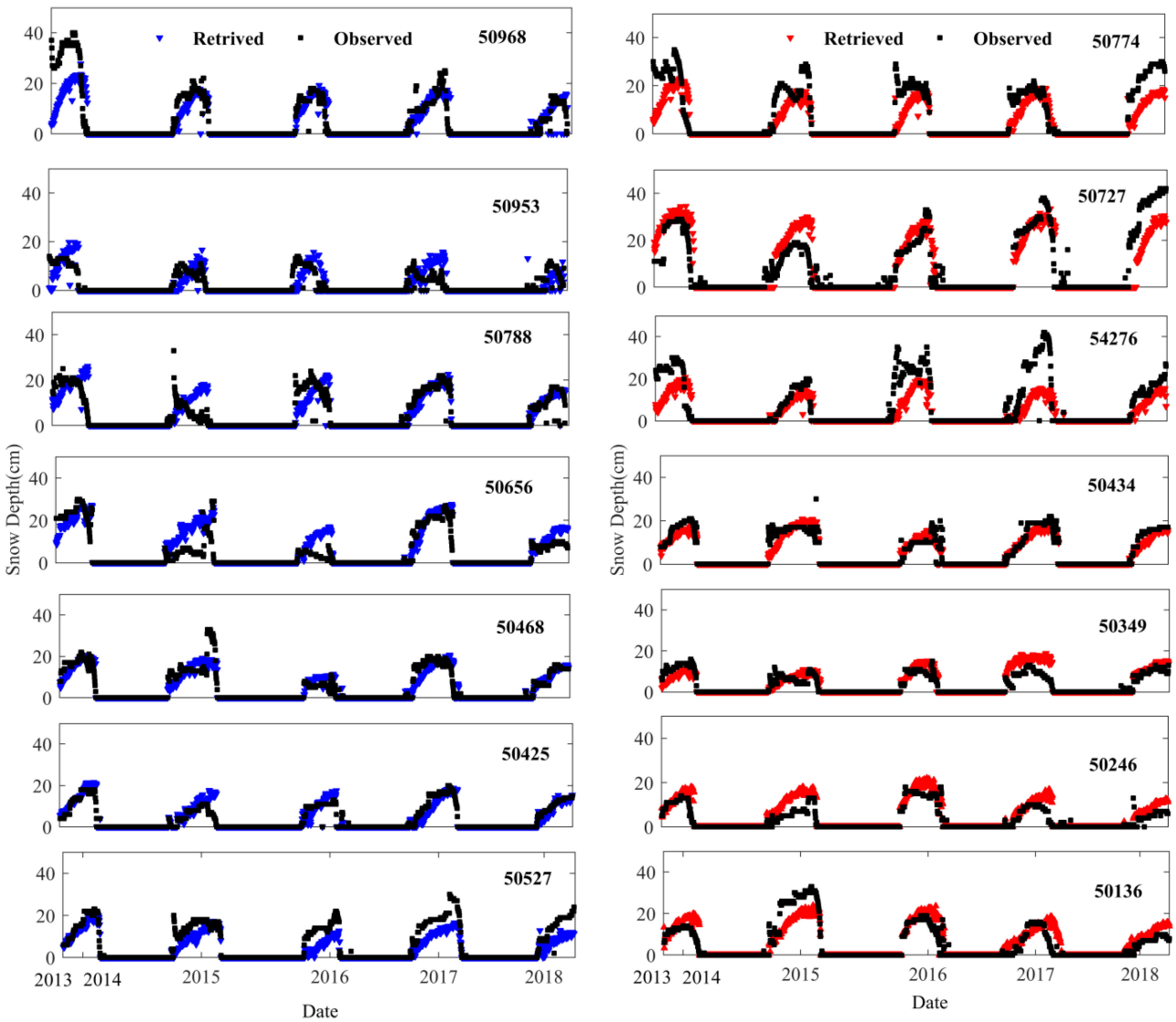

Fig. 6. Comparisons of SD retrieved by the IGAS algorithm and observed at 14 meteorological stations from December 2013 to February 2018: the left represents the nonforest regions and the right represents the forest areas.

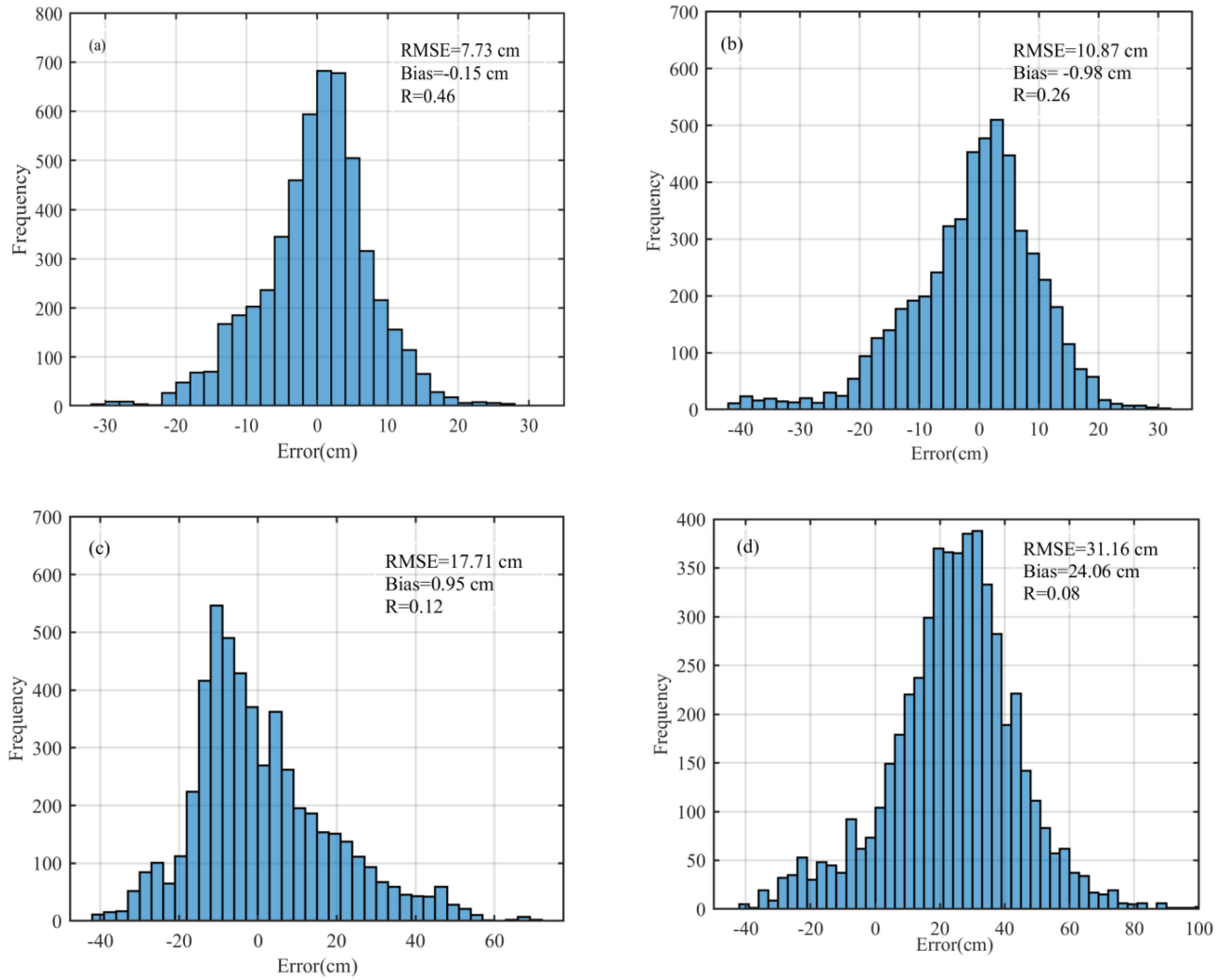

Fig. 7. Error frequency distribution of retrieved SD. The error is equal to the observed SD minus the retrieved SD. (a) IGAS. (b) Che. (c) Chang. (d) AMSR2.

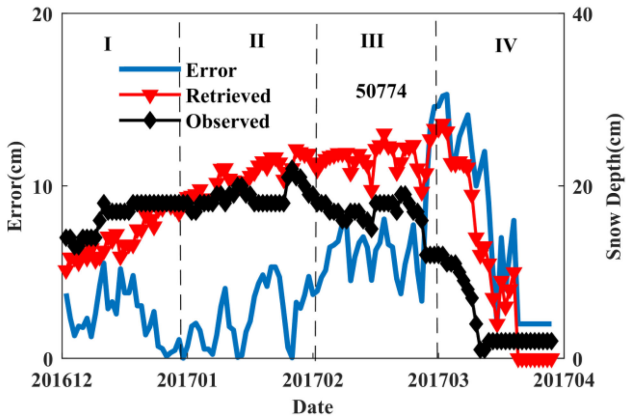

Fig. 8. Error values between the retrieved SD and observed SD at station 50 774 in four snowfall periods I-December; II-January; III-February; and IV-March.

and we calculated the accuracy of four SD inversion algorithms and products in different snowfall periods, whose results were shown in Fig. 9. We could notice that the inversion accuracy had obvious differences in different periods for each SD algorithm and product. For the IGAS algorithm that considered the effect of the variability of snow properties throughout the winter, it had higher inversion accuracy against the other SD products and algorithms. In addition, we also found that the correlation with the observed SD reached minimum in March. The RMSE exceeded 10 cm for the four inversion algorithms and products, and there were obvious overestimations at this time; the reason would be discussed in detail later in the text. However, compared with the other three SD algorithms and products, the IGAS algorithm still had the highest accuracy in the entire snowfall period, although its RMSE and R were 10.45 cm and 0.31 in March, respectively.

B. Effects of Liquid Water Content During Snow Melting Period

From the discussion above, we can conclude that the snow cover metamorphism affected the accuracy of SD inversion. If the metamorphism process of snow cover was not considered, such as the Chang algorithm, a serious error would occur in the

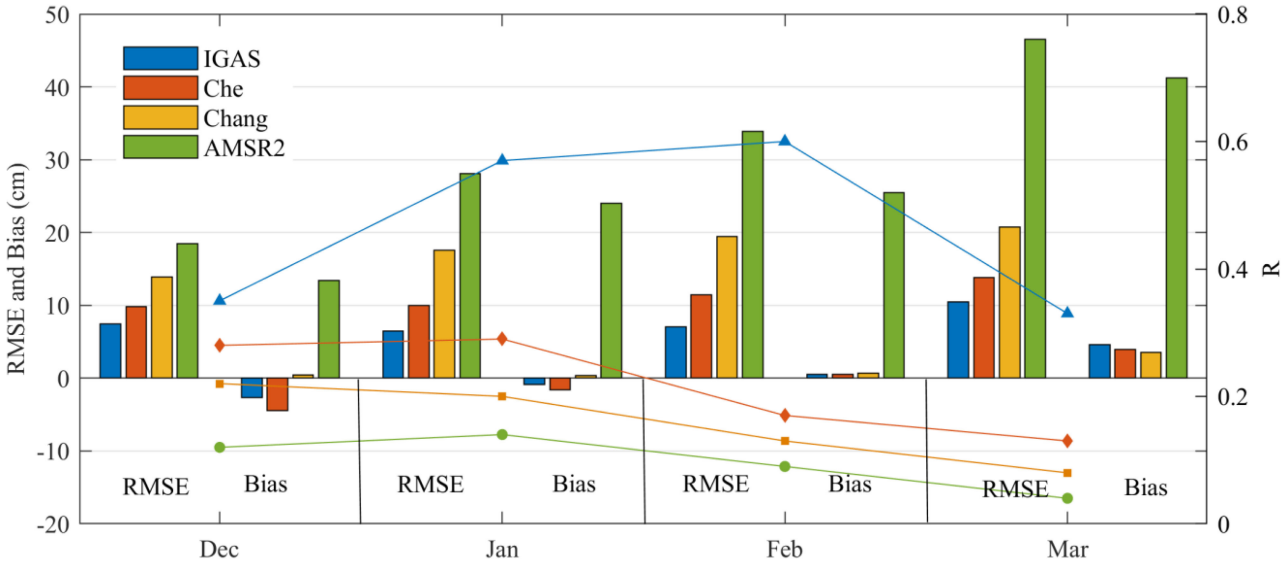

Fig. 9. Monthly RMSE and bias variations in four snow periods. The corresponding lines represent the time series of the correlation coefficient and the impact of different periods on the inversion algorithm.

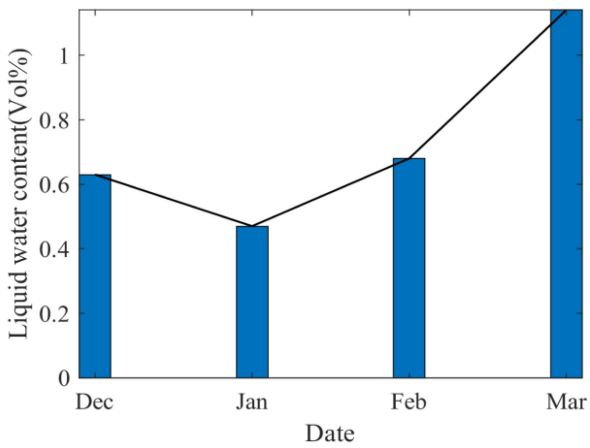

Fig. 10. Volume fraction of liquid water during the entire snow season from snow survey experiments.

process of SD inversion. In this study, snow cover metamorphism had been taken into consideration, and a dynamic coefficient between SD and TBD was given; thus, the IGAS algorithm effectively improved the SD inversion accuracy in different periods. However, the IGAS algorithm had the lowest inversion accuracy in March compared with the other three periods (see Fig. 9). Through snow survey experiments, we found that the liquid water content was the main cause of this error.

Passive microwave can penetrate dry snow and detect the volume scattering signal of snow particles; however, when the snow is wet, the microwave signal changes dramatically [48], [49]. The presence of liquid water in the snow not only absorbed the microwave radiation but also emitted the radiant energy itself. The volume fraction of liquid water was obtained by a snowfork instrument in the snow survey experiment. The statistical results for the entire snow season were shown in Fig. 10. The volume fraction of liquid water exceeded 1% in March, which altered the microwave emission characteristics. Therefore, the brightness temperature of wet snow can only represent information on the snow surface but not the internal structure information of snowpacks, which was a common flaw in the current snow inversion algorithm using microwave signal [49], and of course, including our IGAS algorithm.

C. Impacts of Different Forest Fractions

The accuracy of SD inversion was not only affected by snow metamorphism but also by different underlying surface types, especially in forest areas [50], [51]. From the results in Fig. 5, we could find that compared with the nonforest areas, the inversion results existed an obvious error in forest areas. Therefore, it is necessary to discuss the impact of the forest coverage on the IGAS algorithm. In this section, the SD from dataset 1 in the forest area was used as observed SD, including 87 samples, and their spatial distribution was shown in Fig. 1(b); the forest fraction ranges from 0.1 to 1, and we will discuss from the following two aspects.

1) When only the snow metamorphism over time was considered, and the forest coverage was not considered, i.e., using (7) to perform SD inversion, we obtained the result represented by the blue line in Fig. 11, where the abscissa represented the forest coverage fraction, and the ordinate represented the percentage (%) that the SD inversion result underestimated the observed SD. Fig. 11 illustrated that the retrieved SD based on (7) underestimated the observed SD when the forest fraction exceeds 0.2, and the result was more significant with the increase of forest fraction. In addition, we could also notice that the inversion SD underestimated the observed SD by more than 30% when the forest fraction exceeded 0.8, and it implied that the forest cover had a serious impact on the inversion results.
2) When both the snow metamorphism and forest coverage were considered, i.e., using the IGAS algorithm, the inversion results were shown by the black lines in Fig. 11, and the results showed that the IGAS algorithm also underestimated the observed SD when the forest fraction exceeds

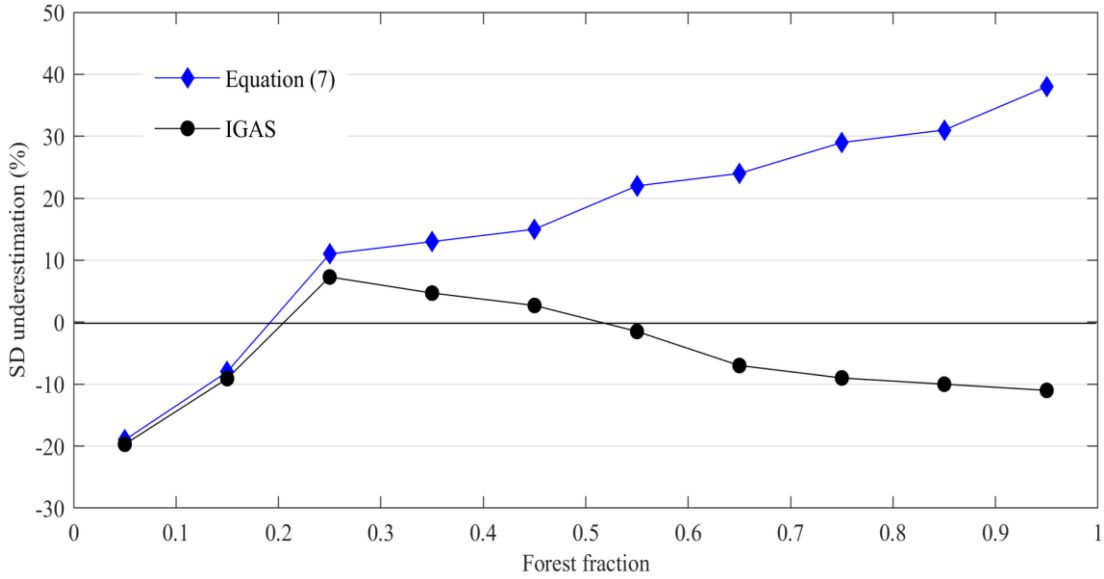

Fig. 11. Impact of different forest coverages.

0.2, but different from (7), it overestimated the observed SD when fraction exceeds 0.5. Although the IGAS algorithm underestimates or overestimates the observed SD, it did not exceed 10% of the total and indicated that the IGAS algorithm could effectively correct the influence of forest on SD retrieval against (7) in which the forest fraction was not considered.

D. Optimization of the Algorithm in the Forest Area

We tried to use different datasets to optimize the IGAS algorithm in the forest regions. From the discussion above, we found that different forest fractions would have a great impact on the inversion results (see Fig. 11). The SD dataset from the meteorological stations was used; however, the meteorological stations were located in the forest area where the forest fraction exceeded 0.7, and the other meteorological stations were located in nonforest areas, where forest coverage was less than 0.2. Due to the uneven distribution of forest cover, it was not suitable to use them for optimizing parameters a and b. Therefore, in this study, a total of 87 snow samples in the forest regions from dataset 1 were used to optimize parameters a and b in (8), and the range of forest fraction was evenly distributed between 0.1 and 1. The results were shown in Fig. 12; the error value between the inversion and the observed SD values was the smallest when the value of a was found to be 0.4 and b was equal to 0.6. Therefore, the value of a and b was taken 0.4 and 0.6 in this article. The observed SD at the meteorological station was used to validate the inversion algorithm (see Fig. 4). The inversion results showed that the optimization method above was reliable when a was set to 0.4 and b was equal to 0.6.

E. Advantages and Limitations of the IGAS Algorithm

The IGAS SD inversion algorithm proposed in this article mainly had the following two advantages. First, the IGAS algorithm used a specific dynamic coefficient to reduce the impact of snow metamorphism and forest attenuation on SD inversion.

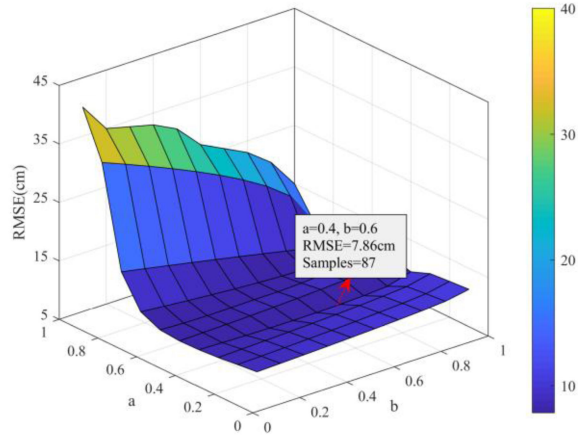

Fig. 12. Optimization of the algorithm in the forest regions.

Although physical models, such as MEMLS [29], could achieve high accuracy and low estimation error, they needed more input parameters that were not easily available. And compared with the physical model, all independent variables in the IGAS algorithm could be easily acquired using passive microwave remote-sensing data, which was conducive to the development of this algorithm into an operating model.

Second, the traditional empirical algorithms, e.g., Chang algorithm and Foster algorithm, only considered the state of the snow layer at a certain moment; however, the effect of structure characteristics of snow cover and the variability of grain size and other snow properties commonly found further complicate the SD relationship to TBD [52]; the traditional empirical algorithm could not achieve high precision. In contrast, the IGAS algorithm considered snow metamorphism by a specific dynamic coefficient and had high accuracy in the whole winter.

Although the proposed algorithm achieved good performance and high accuracy, it still had certain limitations. The IGAS algorithm was developed based on the TBD between two

TABLE IV
COMPARISON OF FOUR SD ALGORITHMS WITH PRODUCTS IN DEEP (> 25 CM) AND SHALLOW (≤ 25 CM) SNOW COVER

	IGAS		Che		Chang		AMSR2	
SD(cm)	⩽25	>25	⩽25	>25	⩽25	>25	⩽25	>25
R	0.65	0.12	0.51	0.08	0.24	0.04	0.15	0.02
RMSE(cm)	6.38	17.74	7..48	20.26	24.25	22.79	31.9	25.20
Bias(cm)	2.43	-15.55	0.41	-17.25	11.21	-11.05	17.41	8.05
Samples	⩽25: 30669(92.5%);			>25: 2505(7.5%)				

microwave bands (18 and 36 GHz). When the snow layer exceeded a certain thickness, the TBD between 18 and 36 GHz would reach saturation; Fig. 4 indicated that the IGAS algorithm does not fully solve the underestimation problems. Fig. 5 also illustrated that the IGAS algorithm had a bad predictive ability for extremely deep snow conditions, especially in the forest area [see Fig. 5(b)]. For deep snow (> 25 cm), the RMSE and bias were up to 17.74 cm and −15.55 cm, respectively, and the R was only 0.12. The other SD algorithms and products, including Che product, Chang algorithm, and AMSR2 SD product, were also analyzed, and the results were given in Table IV; it could be found that the Chang algorithm and AMSR2 SD product had a smaller deviation, their bias was −11.05 and 8.05 cm for deep snow, but their errors were larger, and the RMSE was 22.79 cm for Chang algorithm and 25.20 cm for AMSR2 SD product. We checked dataset 2 and found that deep snow conditions account for approximately 7.5% of all samples, the extreme high SD data (>50 cm) rarely occurred in Northeast China, and the SD was less than 25 cm in most cases. Table IV could be seen that the IGAS algorithm had higher inversion accuracy for shallow snow (≤25 cm), its R, RMSE, and bias were 0.65, 6.38 cm and 2.43 cm, respectively. In addition, numerous studies have been conducted on the snow cover in Northeast China and have indicated that SD estimation in the mountains remains a challenge [7], [29]. Snow properties in mountainous areas vary dramatically in space, making characterization difficult. The IGAS algorithm produced in this study had also a greater uncertainty in the mountains [see Fig. 5(b)], especially for deep snow. Thus, in future works, we attempt to operate the machine learning algorithms, such as the ANN model [53], to overcome the limitations of the traditional TBD approaches.

VI. CONCLUSION

Northeast China is an important commodity grain base, and it is also one of the main snow-covered areas in the world [46]. At present, the traditional empirical and semiempirical algorithms are based on a fixed snow density and snow particle size, and they calibrate the relationship between SD and TBD on the limited dataset. However, the effect of the layered or stratified nature of snow cover and the variability of snow properties commonly found further complicate the SD relationship to TBD. Although physical models could achieve high accuracy and low estimation error, which need more input parameters that are not easily obtained, it is necessary to improve the empirical algorithm (only based on TBD).

In this study, to solve the challenge, a snow survey experiment was designed to quantify a dynamic coefficient based on the MEMLS and snow characteristics in different periods, and then a dynamic SD inversion algorithm for considering snow metamorphism was derived from AMSR2 passive microwave brightness temperature data. Besides, we optimized the forest parameters to overcome the impact of the forest on the microwave signal. The novel SD inversion algorithm proposed in this article, we called the IGAS algorithm, was conducive to the development of this algorithm into an operating model, and it could achieve higher accuracy in the whole winter. Through the statistical analysis, the following conclusions are drawn.

1) The validation results at 98 meteorological stations, including 33 174 samples during the period December 2013–February 2018, showed that the IGAS algorithm achieved better stability in the long term, its RMSE, bias, and R were 7.79 cm, 1.07 cm, and 0.61, respectively. In addition, the IGAS algorithm performed a better correlation with observed SD in nonforest regions, its RMSE, bias, and R were 6.43 cm, 2.43 cm, and 0.69; yet, the RMSE, bias, and R were 9.20 cm, −0.18 cm, and 0.47 in forest regions.
2) The IGAS algorithm could achieve higher accuracy compared with the existing SD algorithms and products, including Che SD product, Chang algorithm, and AMSR2 SD product in the whole winter. Due to the increase in liquid water content over time, the inversion accuracy reached minimum in March. In addition, the IGAS algorithms had a bad predictive ability for extremely deep snow conditions, especially in the forest area. However, deep snow conditions account for approximately 7.5% of all samples, the extreme high SD data (>50 cm) rarely occurred in Northeast China, and the SD was less than 25 cm in most cases (92.5%). Thus, the IGAS algorithm was still applicable for snow monitoring and inversion in Northeast China.
3) The IGAS algorithm provided acceptable results; meanwhile, it was flawed by the limitations of only two frequency bands (18 and 36 GHz) for SD inversion. For example, when the SD exceeded a certain thickness, the scattered microwave signal by the snow particles was

approximately equal to snowpack upwelling thermal radiation as SD gradually increases, which would lead to the retrieved SD based on the IGAS algorithm underestimated the observed SD.

In addition to the influence of snow evolution, some other factors, such as forest type and digital elevation model should also be considered for SD estimation in the mountains. Because of these complexities, the IGAS algorithm produced had high uncertainty in mountainous areas. Thus, in future works, we attempt to operate the machine learning algorithms to overcome the limitations.

ACKNOWLEDGMENT

The authors would like to thank the Science and Technology Basic Resources Survey Project of China for providing snow test data for this article.

REFERENCES

[1] J. Cohen, "Snow cover and climate," *Weather,* vol. 49, no. 5, pp. 150–156, May 1994.

[2] M. New, M. Hulme, and P. Jones, "Representing twentieth-century space–time climate variability—Part II: Development of 1901–96 monthly grids of terrestrial surface climate," *J. Climate*, vol. 13, no. 13, pp. 2217–2238, Jul. 2000.

[3] C. Rixen, C. Schwoerer, and S. Wipf, "Winter climate change at different temporal scales in Vaccinium myrtillus, an Arctic and alpine dwarf shrub," *Polar Res.*, vol. 29, no. 1, pp. 85–94, Apr. 2010.

[4] H. Steltzer, C. Landry, T. H. Painter, J. Anderson, and E. Ayres, "Biological consequences of earlier snowmelt from desert dust deposition in alpine landscapes," in *Proc. Nat. Acad. Sci. USA*, vol. 106, no. 28, pp. 11629–11634, Jul. 2009.

[5] D. A. Robinson, K. F. Dewey, and R. R. Heim, "Global snow cover monitoring: An update," *Bull. Amer. Meteorol. Soc.*, vol. 74, no. 9, pp. 1689–1696, Sep. 1993.

[6] B. Brasnett, "Global analysis of snow depth for numerical weather prediction," *J. Appl. Meteorol.*, vol. 38, no. 6, pp. 726–740, Jun. 1999.

[7] X. Li, K. Zhao, L. Wu, X. Zheng, and T. Jiang, "Spatiotemporal analysis of snow depth inversion based on the FengYun-3B microwave radiation imager: A case study in Heilongjiang province, China," *J. Appl. Remote Sens.*, vol. 8, no. 1, May 2014, Art. no. 084692.

[8] J. L. Foster, D. K. Hall, A. Rango, and A. T. C. Chang, "An overview of passive microwave snow research and results," *Rev. Geophys.*, vol. 22, no. 2, pp. 195–208, May 1984.

[9] K. F. Kunzi, S. Patil, and H. Rott, "Snow-cover parameters retrieved from NIMBUS-7 scanning multichannel microwave radiometer (SMMR) data," *IEEE Trans. Geosci. Remote Sens.*, vol. GE-20, no. 4, pp. 452–467, Oct. 1982.

[10] J. Cohen and D. Rind, "The effect of snow cover on the climate," *J. Climate*, vol. 4, pp. 689–706, Jul. 1991.

[11] C. N. Grody, "Classification of snow cover and precipitation using the special sensor microwave imager," *J. Geophys. Res.*, vol. 96, no. D4, pp. 7423–7435, Apr. 1991.

[12] M. Tedesco and P. S. Narvekar, "Assessment of the NASA AMSR-E SWE product," *IEEE J. Sel. Topics Appl. Earth Observ. Remote Sens.*, vol. 3, no. 1, pp. 141–159, Mar. 2010.

[13] X. Zou, J. Zhao, F. Weng, and Z. Qin, "Detection of radio-frequency interference signal over land from FY-3B microwave radiation imager (MWRI)," *IEEE Trans. Geosci. Remote Sens.,* vol. 50, no. 12, pp. 4994–5003, Dec. 2012.

[14] E. Cho, S. E. Tuttle, and J. M. Jacobs, "Evaluating consistency of snow water equivalent retrievals from passive microwave sensors over the North Central U.S.: SSM/I vs. SSMIS and AMSR-E vs. AMSR2," *Remote Sens.*, vol. 9, no. 5, May 2017, Art. no. 465.

[15] J. L. Foster *et al.*, "A blended global snow product using visible, passive microwave and scatterometer satellite data," *Int. J. Remote Sens.,* vol. 32, no. 5, pp. 1371–1395, Mar. 2011.

[16] Y. Liu *et al.*, "Assimilating satellite-based snow depth and snow cover products for improving snow predictions in Alaska," *Adv. Water Resour.*, vol. 54, pp. 208–227, Apr. 2013.

[17] M. Ruedi, N. Weyeneth, E. C. Teeling, S. Puechmaille, and S. M. Goodman, "Biogeography of old world emballonurine bats (Chiroptera: Emballonuridae) inferred with mitochondrial and nuclear DNA," *Mol. Phylogenetics Evol.,* vol. 64, no. 1, pp. 204–211, Apr. 2012.

[18] A. T. C. Chang, J. L. Foster, D. K. Hall, A. Rango, and B. K. Hartline, "Snow water equivalent estimation by microwave radiometry," *Cold Regions Sci. Technol.,* vol. 5, no. 3, pp. 259–267, Mar. 1982.

[19] L. Jiang, P. Wang, L. Zhang, H. Yang, and J. Yang, "Improvement of snow depth retrieval for FY3B-MWRI in China," *Sci. China Earth Sci.,* vol. 57, no. 6, pp. 1278–1292, Jun. 2014.

[20] K. S. Chen, T.-D. Wu, L. Tsang, Q. Li, J. Shi, and A. K. Fung, "Emission of rough surfaces calculated by the integral equation method with comparison to three-dimensional moment method simulations," *IEEE Trans. Geosci. Remote Sens.*, vol. 41, no. 1, pp. 90–101, Jan. 2003.

[21] L. Dai, T. Che, J. Wang, and P. Zhang, "Snow depth and snow water equivalent estimation from AMSR-E data based on a priori snow characteristics in Xinjiang, China," *Remote Sens. Environ.*, vol. 127, pp. 14–29, Dec. 2012.

[22] X. Xiao, T. Zhang, X. Zhong, W. Shao, and X. Li, "Support vector regression snow-depth retrieval algorithm using passive microwave remote sensing data," *Remote Sens. Environ.,* vol. 210, pp. 48–64, Jun. 2018.

[23] I. J. Davenport, M. J. Sandells, and R. J. Gurney, "The effects of variation in snow properties on passive microwave snow mass estimation," *Remote Sens. Environ.,* vol. 118, no. pp. 168–175, Mar. 2012.

[24] J. L. Foster, A. T. C. Chang, and D. K. Hall, "Comparison of snow mass estimates from a prototype passive microwave snow algorithm, a revised algorithm and a snow depth climatology," *Remote Sens. Environ.*, vol. 62, no. 2, pp. 132–142, Nov. 1997.

[25] E. G. Josberger and N. M. Mognard, "A passive microwave snow depth algorithm with a proxy for snow metamorphism," *Hydrol. Processes,* vol. 16, no. 8, pp. 1557–1568, Jun. 2002.

[26] T. Che, X. Li, R. Jin, R. Armstrong, and T. Zhang, "Snow depth derived from passive microwave remote-sensing data in China," *Ann. Glaciol.,* vol. 49, no. 1, pp. 145–154, Oct. 2008.

[27] R. Kelly, "The AMSR-E snow depth algorithm: Description and initial results," *J. Remote Sens. Soc. Jpn.*, vol. 29, no. 1, pp. 307–317, Jan. 2009.

[28] Y. Wei, X. Li, K. Zhao, and L. Gu, "An improved snow depth retrieval algorithm for AMSR2 passive microwave data based on snow survey data in Northeast China," in *Proc. Photon. Electromagn. Res. Symp.,* 2019, pp. 1469–1476.

[29] T. Che, L. Dai, X. Zheng, X. Li, and K. Zhao, "Estimation of snow depth from passive microwave brightness temperature data in forest regions of Northeast China," *Remote Sens. Environ.*, vol. 183, pp. 334–349, Sep. 2016.

[30] Q. Li *et al.*, "The influence of thermal properties and canopy-intercepted snow on passive microwave transmissivity of a scots pine," *IEEE Trans. Geosci. Remote Sens.*, vol. 57, no. 8, pp. 5424–5433, Aug. 2019.

[31] Q. Li and R. E. J. Kelly, "Correcting satellite passive microwave brightness temperatures in forested landscapes using satellite visible reflectance estimates of forest transmissivity," *IEEE J. Sel. Topics Appl. Earth Observ. Remote Sens.,* vol. 10, no. 9, pp. 3874–3883, Sep. 2017.

[32] J. Yang, L. Jiang, S. Wu, G. Wang, J. Wang, and X. Liu, "Development of a snow depth estimation algorithm over China for the FY-3D/MWRI," *Remote Sens.*, vol. 11, no. 8, Apr. 2019, Art. no. 977.

[33] Y. Zhang, D. Guan, C. Jin, A. Wang, J. Wu, and F. Yuan, "Analysis of impacts of climate variability and human activity on streamflow for a river basin in Northeast China," *J. Hydrol.*, vol. 410, no. 3/4, pp. 239–247, Nov. 2011.

[34] Y. Zhao *et al.*, "Long-term land cover dynamics (1986–2016) of Northeast China derived from a multi-temporal Landsat archive," *Remote Sens.*, vol. 11, no. 5, Mar. 2019, Art. no. 599.

[35] X. Li, S. Liang, and K. Zhao, "Snow cover classification based on climate variables and its distribution characteristics in China," *J. Glaciol. Geocryol.,* vol. 41, no. 4, pp. 1–10, 2019.

[36] M. Sturm, J. Holmgren, and G. E. Liston, "A seasonal snow cover classification system for local to global applications," *J. Climate*, vol. 8, no. 5, pp. 1261–1283, May 1995.

[37] Y. He and Y. Bo, "A consistency analysis of MODIS MCD12Q1 and MERIS globcover land cover datasets over China," in *Proc. Int. Conf. Geoinform.,* 2011, pp. 1–6.

[38] J. Wang *et al.*, "Investigation on snow characteristics and their distribution in China," *Adv. Earth Sci.,* vol. 33, no. 1, pp. 12–26, 2018.

[39] C. H. E. Tao, "Long-term series of daily snow depth dataset in China (1979–2019)," Nat. Tibetan Plateau Data Center, Beijing, China, 2015.
[40] N. C. Grody and A. N. Basist, "Global identification of snowcover using SSM/I measurements," *IEEE Trans. Geosci. Remote Sens.,* vol. 34, no. 1, pp. 237–249, Jan. 1996.
[41] A. Wiesmann and C. Mätzler, "Microwave emission model of layered snowpacks," *Remote Sens. Environ.,* vol. 70, no. 3, pp. 307–316, Dec. 1999.
[42] T. Markus, D. C. Powell, and J. R. Wang, "Sensitivity of passive microwave snow depth retrievals to weather effects and snow evolution," *IEEE Trans. Geosci. Remote Sens.*, vol. 44, no. 1, pp. 68–77, Jan. 2006.
[43] C. Mätzler and A. Wiesmann, "Extension of the microwave emission model of layered snowpacks to coarse-grained snow," *Remote Sens. Environ.*, vol. 70, no. 3, pp. 317–325, Dec. 1999.
[44] C. Mätzler, "Relation between grain-size and correlation length of snow," *J. Glaciol.*, vol. 48, no. 162, pp. 461–466, Jan. 2002.
[45] R. E. Davis and J. Dozier, "Stereological characterization of dry Alpine snow for microwave remote sensing," *Adv. Space Res.*, vol. 9, no. 1, pp. 245–251, Dec. 1989.
[46] L. Gu, X. Fan, X. Li, and Y. Wei, "Snow depth retrieval in farmland based on a statistical lookup table from passive microwave data in Northeast China," *Remote Sens.,* vol. 11, no. 24, Dec. 2019, Art. no. 3037.
[47] J. Wang, X. Huang, Y. Wang, and T. Liang, "Retrieving snow depth information from AMSR2 data for Qinghai-Tibet plateau," *IEEE J. Sel. Topics Appl. Earth Observ. Remote Sens.*, vol. 13, pp. 752–768, Feb. 2020.
[48] A. E. Walker and B. E. Goodison, "Discrimination of a wet snow cover using passive microwave satellite data," *Ann. Glaciol.,* vol. 17, pp. 307–311, 1993.
[49] T. Che, X. Li, R. Jin, and C. Huang, "Assimilating passive microwave remote sensing data into a land surface model to improve the estimation of snow depth," *Remote Sens. Environ.,* vol. 143, pp. 54–63, Mar. 2014.
[50] N. R. Hedstrom and J. W. Pomeroy, "Measurements and modelling of snow interception in the boreal forest," *Hydrol. Processes*, vol. 12, no. 10/11, pp. 1611–1625, Aug./Sep. 1998.
[51] R. D. De Roo, A. R. Chang, and A. W. England, "Radiobrightness at 6.7-, 19-, and 37-GHz down welling from mature evergreen trees observed during the cold lands processes experiment in Colorado," *IEEE Trans. Geosci. Remote Sens.*, vol. 45, no. 10, pp. 3224–3229, Oct. 2007.
[52] D. Li, M. Durand, and S. A. Margulis, "Potential for hydrologic characterization of deep mountain snowpack via passive microwave remote sensing in the Kern river basin, Sierra Nevada, USA," *Remote Sens. Environ.,* vol. 125, pp. 34–48, Oct. 2012.
[53] E. Santi *et al.*, "Monitoring of Alpine snow using satellite radiometers and artificial neural networks," *Remote Sens. Environ.,* vol. 144, pp. 179–186, Mar. 2014.

Yanlin Wei received the bachelor's degree in electronic and information engineering from BaiCheng Normal College, Baicheng, China, in 2018. He is currently working toward the M.S. degree in electromagnetic field and microwave technology at Jilin University, Changchun, China.

He is currently studying with the Northeast Institute of Geography and Agroecology, Chinese Academy of Sciences, Changchun, China. His research interests include passive microwave remote sensing on snow, snow depth inversion, and modeling.

Xiaofeng Li (Member, IEEE) received the B.Sc. and M.Sc. degrees in mathematics from Jilin University, Changchun, China, in 2002 and 2005, respectively, and the Ph.D. degree in remote sensing and geosciences from the Chinese Academy of Sciences, Changchun, China, in 2008.

He is currently a Professor with the Research Center of Remote Sensing and Geoscience, Northeast Institute of Geography and Agroecology, Chinese Academy of Sciences. He is also the Chair of the IEEE GRSS Changchun chapter. His current research interest focuses on the snow parameters inversion by remote sensing data, image processing, and agriculture remote sensing. He has authored or coauthored more than 50 papers in journals and conference proceedings.

Lingjia Gu (Member, IEEE) received the Ph.D. degree in electrical circuits and systems from Jilin University, Changchun, China, in 2008.

She is currently a Professor with the College of Electronic Science and Engineering, Jilin University, Changchun, China. From 2010 to 2012, she held a Postdoctoral Research with the Northeast Institute of Geography and Agroecology, Chinese Academy of Sciences, China. Her current research interests include remote sensing data processing and digital image processing.

Xingming Zheng (Member, IEEE) received the Ph.D. degree in cartography and geographic information system from the Northeast Institute of Geography and Agroecology, Chinese Academy of Sciences, Changchun, China, in 2012.

Since July 2012, he has been a Research Associate with the Northeast Institute of Geography and Agroecology, Chinese Academy of Sciences. His research interests include passive microwave remote sensing of soil moisture, geophysical inversion model, microwave radiative/scattering transfer model, and its application on crop canopy.

Tao Jiang (Member, IEEE) received the Ph.D. degree in cartography and geographic information system from the Northeast Institute of Geography and Agroecology, Chinese Academy of Sciences, Changchun, China, in 2019.

He is currently an Engineer with Microwave Remote Sensing Group, Research Center of Remote Sensing and Geoscience, Northeast Institute of Geography and Agroecology, Chinese Academy of Sciences. His research interests include microwave radiometer design and the development and detection of radio frequency interference.

Xiaojie Li (Member, IEEE) received the Ph.D. degree in optical engineering from Tianjin University, Tianjin, China, in 2010.

She is currently an Associate Professor with the Northeast Institute of Geography and Agroecology, Chinese Academy of Sciences, Changchun, China. Her research interests include photoelectric detection technology and remote sensing data processing and high-performance computing.

Xiangkun Wan received the bachelor's degree in electronic and information engineering from Jilin University, Changchun, China, in 2015. He is currently working toward the Ph.D. degree in cartography and geography information system at the University of the Chinese Academy of Sciences, Beijing, China.

His research interests include microwave radiometer design and droneborne radiometer design.